Available online at www.sciencedirect.com
SCIENCE DIRECT®
Biomaterials 26 (2005) 4817–4827
Biomaterials
www.elsevier.com/locate/biomaterials

Bone tissue engineering using polycaprolactone scaffolds fabricated via selective laser sintering

Jessica M. Williams[a], Adebisi Adewunmi[b], Rachel M. Schek[a,c], Colleen L. Flanagan[a], Paul H. Krebsbach[a,c], Stephen E. Feinberg[d], Scott J. Hollister[a,b,e], Suman Das[b,*]

[a]Department of Biomedical Engineering, University of Michigan, Ann Arbor, Michigan 48109-2125, USA
[b]Department of Mechanical Engineering, University of Michigan, 2250 GG Brown Bldg, 2350 Hayward St., Ann Arbor, Michigan 48109-2125, USA
[c]Oral Medicine, Pathology, and Oncology, School of Dentistry, Ann Arbor, Michigan 48109-1078, USA
[d]Department of Oral and Maxillofacial Surgery, University of Michigan, Ann Arbor, Michigan 48109-0018, USA
[e]Department of Surgery, The University of Michigan, Ann Arbor, Michigan 48109-0329, USA

Received 16 July 2004; accepted 8 November 2004
Available online 23 January 2005

Abstract

Polycaprolactone (PCL) is a bioresorbable polymer with potential applications for bone and cartilage repair. In this work, porous PCL scaffolds were computationally designed and then fabricated via selective laser sintering (SLS), a rapid prototyping technique. The microstructure and mechanical properties of the fabricated scaffolds were assessed and compared to the designed porous architectures and computationally predicted properties. Scaffolds were then seeded with bone morphogenetic protein-7 (BMP-7) transduced fibroblasts and implanted subcutaneously to evaluate biological properties and to demonstrate tissue in-growth. The work done illustrates the ability to design and fabricate PCL scaffolds with porous architecture that have sufficient mechanical properties for bone tissue engineering applications using SLS. Compressive modulus and yield strength values ranged from 52 to 67 MPa and 2.0 to 3.2 Mpa, respectively, lying within the lower range of properties reported for human trabecular bone. Finite element analysis (FEA) results showed that mechanical properties of scaffold designs and of fabricated scaffolds can be computationally predicted. Histological evaluation and micro-computed tomography (μCT) analysis of implanted scaffolds showed that bone can be generated in vivo. Finally, to demonstrate the clinical application of this technology, we designed and fabricated a prototype mandibular condyle scaffold based on an actual pig condyle. The integration of scaffold computational design and free-form fabrication techniques presented here could prove highly useful for the construction of scaffolds that have anatomy specific exterior architecture derived from patient CT or MRI data and an interior porous architecture derived from computational design optimization.

Keywords: Bone tissue engineering; Finite element analysis; Laser manufacturing; Mechanical properties; Micro-computed tomography (μCT); Polycaprolactone; Porosity; Rapid prototyping; Solid free-form fabrication

1. Introduction

Repair and reconstruction of complex joints such as the temporo-mandibular joint (TMJ) pose many challenges for bone tissue engineering. Adverse reactions to alloplastic, non-biological materials result in compromised functional outcome in patients and autogenous grafts require bone grafting from other parts of the body, which can lead to complications elsewhere in the patient [1,2]. Tissue engineering may overcome these limitations, but to be effective, the scaffolds employed must fit into the anatomic defect, possess mechanical properties that will bear in vivo loads, enhance tissue in-growth, and produce biocompatible degradation

*Corresponding author. Tel.: +1 734 615 6646; fax: +1 734 647 3170.
E-mail address: sumandas@umich.edu (S. Das).

0142-9612/$ - see front matter © 2005 Elsevier Ltd. All rights reserved.
doi:10.1016/j.biomaterials.2004.11.057

byproducts [3–6]. This may be best achieved by combining image-based computational design techniques and solid free-form fabrication (SFF) methods. One such SFF method, selective laser sintering (SLS), may be advantageous for creating bone tissue engineering constructs for sites such as the TMJ, because it provides a cost-effective, efficient method by which to construct scaffolds to match the complex anatomical geometry of craniofacial or periodontal structures, where preformed materials might be difficult and ineffective [2]. The work presented here is one of the first reported efforts on the design, manufacture and characterization of PCL scaffolds by SLS.

Solid free-form fabrication techniques enable design and fabrication of anatomically shaped scaffolds with varying internal architectures, thereby allowing precise control over pore size, porosity, permeability, and stiffness. Control over these characteristics may enhance cell infiltration and mass transport of nutrients and metabolic waste throughout the scaffold. SFF also allows for the fabrication of biphasic scaffolds that incorporate multiple geometries into a single scaffold [7], allowing for in-growth of multiple tissues into a single scaffold structure. Several authors have reviewed the advantages of SFF techniques currently in use [8–12].

SLS constructs scaffolds from 3-D digital data by sequentially fusing regions in a powder bed, layer by layer, via a computer controlled scanning laser beam [13,14]. SLS provides many benefits for fabricating tissue engineering scaffolds that other SFF methods, such as fused deposition modeling (FDM), three-dimensional printing (3DP), stereolithography, or ink-jet printing, may lack. Layer-by-layer additive fabrication in SLS allows construction of scaffolds with complex internal and external geometries. Second, virtually any powdered biomaterial that will fuse but not decompose under a laser beam can be used to fabricate scaffolds. Additionally, SLS does not require the use of organic solvents, can be used to make intricate biphasic scaffold geometries, and does not require the use of a filament (as in FDM). It may be easier to incorporate multiple materials; it is fast and cost effective, making it a well-adapted technology for the fabrication of tissue engineering scaffolds [15–19]. We have employed SLS to create scaffolds in polycaprolactone.

Polycaprolactone (PCL) is a bioresorbable polymer with potential applications for bone and cartilage repair. With respect to SLS, PCL has certain advantages relative to other polymers such as PLA (poly lactic acid). PCL is more stable in ambient conditions, it is significantly less expensive and is readily available in large quantities. Much research is currently focused on the use of PCL biocomposites and co-polymers of PCL with both natural and synthetic polymers [20–30]. PCL scaffolds have previously been created with a variety of SFF techniques including FDM [8,31–34], photopolymerization of a synthesized PCL macromer [26], shape deposition modeling [29], precision extruding deposition [35], 3DP [36], low-temperature deposition [37] and multi-nozzle free-form deposition [11–12,35,38]. However, the fabrication and characterization of PCL scaffolds with varying internal architectures and porosities made through SLS has not been reported.

We have proposed the use of PCL scaffolds fabricated using SLS to engineer bone tissue. If PCL scaffolds are to be successfully utilized for bone tissue engineering, they must be accurately constructed from computational designs, have mechanical properties within an appropriate physiological range, and support the in-growth of bone tissue. Therefore, we have manufactured scaffolds in a variety of designs and then evaluated the microstructure using micro-computed tomography (μCT) and the mechanical properties using compression testing and finite element analysis (FEA). We then evaluated the biological properties of these scaffolds by seeding them with bone morphogenetic protein-7 (BMP-7) transduced human fibroblasts and evaluated the generated tissue using μCT and histology. Finally, to demonstrate the clinical potential of this technology, we employed image-based design techniques to superimpose computed tomography (CT) data with a designed porous architecture to build a complex scaffold that mimics a mandibular condyle. Results show that manufactured scaffolds matched the designs well, had compressive strength and modulus values within the range of trabecular bone, and supported the in-growth of bone in an in vivo model.

2. Materials and methods

2.1. Porous scaffold design and fabrication

Cylindrical porous scaffolds (12.7 mm diameter, 25.4 mm height), with three-dimensional orthogonal periodic porous architectures, were designed using Unigraphics NX 3-D solid modeling software (UGS PLM Solutions, Plano, TX). The designs were then exported to a Sinterstation 2000™ machine (3D Systems, Valencia, CA) in STL file format, and were used to construct scaffolds by SLS processing of ε-polycaprolactone powder (CAPA 6501, Solvay Caprolactones, Warrington, Cheshire, UK). This particular form of PCL has a melting point of 60 °C, a molecular weight of 50,000 Da, and particle size distribution in the 10–100 μm range. SLS processing of the PCL powder was conducted by preheating the powder to 49.5 °C and scanning the laser (450 μm focused beam diameter) at 4.5 W power and 1.257 m/s (49.5 in/s) scan speed. Scaffolds were built layer-by-layer using a powder layer

thickness of 100 μm. After SLS processing was completed, the scaffolds were allowed to cool inside the machine process chamber for approximately 1 h and were then removed from the part bed. Excess powder surrounding the scaffolds was brushed off and the scaffolds were finally cleaned by blowing compressed air and physically removing unsintered powder from the scaffold interstices by insertion of a 1 mm diameter wire.

Six different periodic porous architecture designs were created and 7 specimens for each design were manufactured for microstructure analysis and mechanical testing. The orthogonal pores ranged from 1.75–2.5 mm in diameter, producing scaffolds with designed volumetric porosity ranging from 63 to 79% as calculated from the STL files (see Table 1). Seven solid cylindrical specimens were also created to determine the bulk properties of the SLS manufactured scaffolds. The x/y direction of the scaffolds is defined as being perpendicular to the longitudinal axis (25.4 mm), and the z direction is defined as being parallel to the longitudinal axis of the scaffold.

Six cylindrical porous scaffolds (5.0 mm diameter, 4.5 mm height) were designed and manufactured for in vivo testing (Fig. 7a). These scaffolds were designed to have 1.5 mm diameter orthogonal interconnected pores (porosity = 68%).

2.2. Microstructure analysis

Two specimens from each experimental group ($n = 7$) were scanned in air using a MS-130 high resolution μCT scanner (GE Medical Systems, Toronto, CAN) at 28 μm voxel resolution, at 75 kV and 75 mA. The porosity of each specimen was calculated by defining a region of interest that encompassed the entire scaffold and an appropriate threshold level to delineate the solid PCL material using GEMS Microview software (GE Medical Systems, Toronto, CAN).

2.3. Experimental mechanical property assessment

Seven specimens from each experimental group, including the two that were used for microstructure analysis, were mechanically tested in compression using an MTS Alliance RT30 electromechanical test frame (MTS Systems Corp., MN). The specimens were compressed to failure in the z-direction between two fixed steel platens at a rate of 1 mm/min (ASTM D695-02a) after a preload of 1 lb. was applied.

TestWorks4 software (MTS Systems Corp., MN) was used to collect and analyze data during compression testing. Load and displacement data were recorded. Compressive modulus and compressive yield strength were calculated using area measurements derived from caliper measurements of pre-tested samples. Compressive modulus was defined as the slope of the linear portion of the stress–strain curve. Compressive yield strength was defined as the load carried at the yield point (0.2% offset) divided by the original cross-sectional area of the scaffold.

2.4. Image-based FEA

Complete anisotropic effective stiffness constants were calculated using the voxel-based homogenization software VOXELCON (Quint Corp, Tokyo, Japan). The method creates large-scale finite element meshes by directly meshing voxel datasets from the μCT scans thereby capturing any fabrication feature in the resolution range of the CT scan. Voxel models were created of both the design input STL file and the corresponding voxelized μCT scans for each scaffold design. The STL files were first converted to VOX files in VOXELCON, and then converted to JPEG format using a custom routine written in IDL 5.5 (Research Systems Inc, Boulder, CO). Microview was then used to select a repeating periodic region of interest (ROI) within the

Table 1
Solid modeling design parameters for the orthogonal pores in the x/y and z directions are shown with corresponding design porosities

Design parameters			Design scaffolds	Actual scaffolds			
Pore size (mm)		Porosity (%)	Computational E (Mpa)	Porosity ($n = 2$) (%)	Experimental ($n = 7$)		Computational ($n = 2$) E (MPa)
x/y	z				E (MPa)	σ^y (MPa)	
1.75	1.75	63.1	22.5	37.5±1.5	65±3	3.2±0.5	57±7
2	2	69.3	17.2	46.2±0.2	52±2	2.2±0.1	53±3
1.75	2	69.2	21.1	41.7±0.8	63±4	2.8±0.1	68±4
1.75	2.25	74.5	20.7	45.5±0.1	67±4	2.9±0.2	62±8
2	2.25	74.2	17.3	50.2±0.1	55±3	2.3±0.1	48±1
2	2.5	79.0	16.1	55±0.9	54±3	2.0±0.1	46±3
Solid		0.0	120.0	17.8±0.7	122±13	11.7±0.5	112±12

Computational compressive modulus (E) was calculated for each scaffold design by performing FEA on each design's STL file. Actual scaffold porosities and mechanical properties of the seven different scaffold architectures are also shown. Experimental modulus and yield strength values were calculated through unconfined compression testing. Computational modulus values were calculated by performing FEA on μCT scans of the scaffolds.

STL file, and to export the ROI in PNG image format. A second custom routine written in IDL 5.5 was used to remove noise from the ROI and to convert the ROI to an image in RAW format. This image was imported into VOXELCON for FEA. The μCT scanned scaffold images were imported into Microview and two ROIs, one from the top of the scaffold, and one from the bottom of the scaffold, were selected due to inhomogeneity of the scaffold. The bottom/top designation corresponds to the orientation of the scaffold during the SLS build. The ROIs were exported in PNG format and the same sequence of routines was performed on them as was performed on the STL files. For the FEA, PCL material properties were assumed isotropic with a Young's modulus of 120 MPa (solid material property reported by the manufacturer) and a Poisson's ratio of 0.3.

2.5. Cell seeding and implantation

Primary human gingival fibroblasts (HGF) were prepared from explants of human surgical waste in compliance with the University of Michigan Institutional Review Board [2]. Passage 4 fibroblasts were infected with AdCMV-BMP-7, a recombinant adenovirus construct expressing the murine BMP-7 gene under a cytomegalovirus (CMV) promoter [39]. Such infected primary cells have been shown to form bone in vivo [40–43]. Two million cells were seeded into each scaffold by suspending them in 30 μl of 2 mg/ml collagen gel made from acid-solubilized rat tail collagen (BD Biosciences, Bedford, MA), which was gelled using 37 °C incubation [44]. Six scaffolds with an orthogonal interconnected pore design (pore size = 1.5 mm, porosity = 68%) were manufactured as described previously, seeded with cells, and implanted in 5 to 8 week old immunocompromised mice (N:NIH-bg-nu-xid, Charles River, Wilmington, MA). Animals were anesthetized with injections of ketamine/xylazine (50 and 5 μg/g, respectively), subcutaneous pockets were created, four scaffolds were inserted into each mouse and surgical sites were closed with wound clips in compliance with University Committee on Use and Care of Animals (UCUCA) regulations.

The animals were sacrificed 4 weeks after implantation. The harvested implants were fixed using Z-Fix (Anatech, Battle Creek, MI) and stored in 70% ethanol for μCT analysis. Specimens were scanned in water using a MS-130 high-resolution μCT scanner at 16 μm voxel resolution, at 75 kV and 75 μA. Three-dimensional isosurface renderings of the mineralized tissue were made using MicroView to visualize the remaining scaffold and the generated tissue. The reconstructed three-dimensional data sets were used to calculate the volume of bone present on the scaffolds and the average density of the new bone using MicroView's automated image analysis and thresholding features to define the bone. Following μCT scanning, the scaffolds were demineralized using RDO (APEX Engineering Products Corp, Plainfield, IL). The scaffolds were then embedded in paraffin, sectioned at 7 μm, and stained with hematoxylin and eosin (H&E).

2.6. Mandibular condyle design and fabrication

In order to provide a proof of concept, a minipig condyle scaffold was designed using image-based techniques [45]. A global anatomic design was first created directly from a CT scan of the minipig mandible. A ramus attachment collar was then digitally added using specially written software. The scaffold microstructure, consisting of interconnected cylindrical pores, was also created using specially written image-based design software [46]. The global anatomic condyle design image database was then combined with the scaffold architecture design image database using Boolean operations. The final result was a porous, anatomically shaped mandibular condyle scaffold that can be attached to the mandibular ramus via the designed collar.

3. Results

3.1. Micro-structure analysis

Terminology: Volume fraction refers to the percentage fraction of the entire scaffold volume (12.7 mm diameter × 25.4 mm height) that is occupied by PCL material, whereas porosity refers to the percentage fraction of voids in the entire scaffold volume.

A representative image of the STL file used to manufacture a scaffold, and a porous cylindrical scaffold fabricated by SLS illustrate our ability to manufacture designed scaffolds (Fig. 1).

Porous PCL scaffolds were designed and fabricated with six different internal pore architectures and porosities (Table 1). Designed pore diameter in the x, y direction was 1.75 or 2.0 mm. Designed pore diameter in the z direction ranged from 1.75 to 2.50 mm. Resultant design porosities (Table 1) ranged from 63% to 79%. Micro-CT images were used to visualize the manufactured scaffolds and assess their porosity (Fig. 2b). The designed and actual scaffold porosities were well correlated and directly related with a slope of nearly 1 (Fig. 3). However, the least-squares regression fit does not pass through the origin, illustrating that the manufactured porosity is consistently 27% less than the design porosity for the porous scaffolds (Table 1). The solid cylindrical scaffold had a design porosity of 0% and an actual porosity of 17.8%.

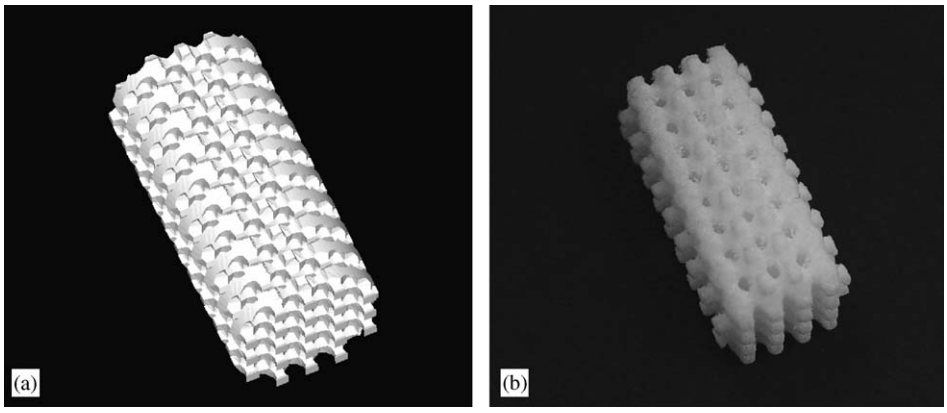

Fig. 1. (a) STL design file for the 1.75 mm $x/y/z$ porous scaffold. (b) 1.75 mm $x/y/z$ PCL scaffold fabricated by SLS.

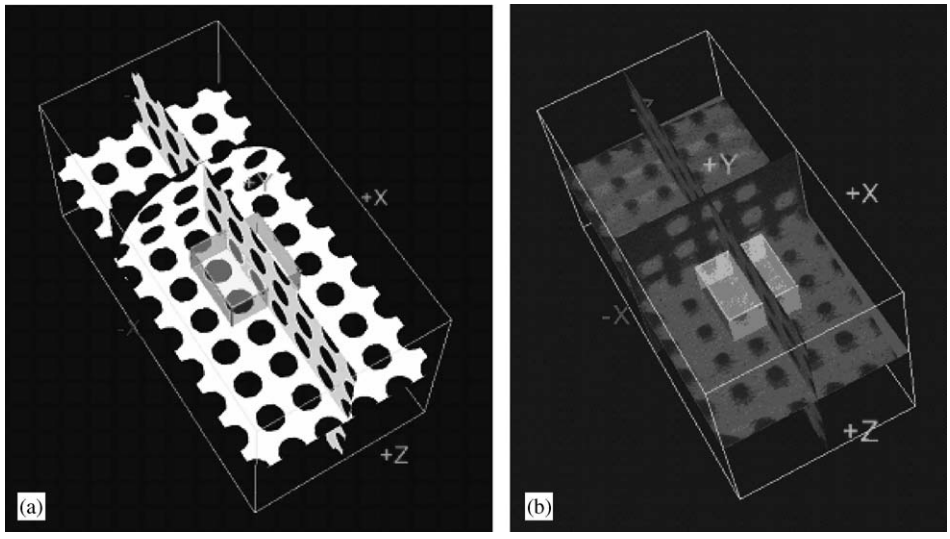

Fig. 2. (a) A voxel rendering of the scaffold's STL file was used to perform FEA on the designed architecture. (b) A voxel rendering of the scaffold's μCT structure was used for volume fraction calculations and for performing FEA on the actual scaffold.

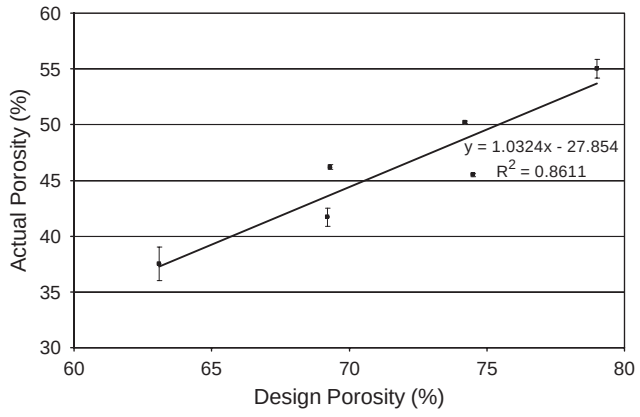

Fig. 3. Correlation between targeted scaffold design porosities and actual scaffold porosities measured by μCT. A least-squares regression line is fit to the data to show correlation.

3.2. Experimental mechanical property assessment

The mechanical properties of the PCL scaffolds designed for this study are reported in Table 1 where "experimental" values are those calculated from compression testing and "computational" results are those produced by FEA on the design files (for design parameters) or on μCT images of the scaffolds (for actual scaffolds). Mean experimental and computational compressive modulus values for the porous scaffolds fell within the lower range of human trabecular bone [47], varying from 52 to 67 MPa and 46 to 68 Mpa, respectively (Table 1). Mean experimental yield strength data also fell within the lower range of human trabecular bone, varying from 2.0 to 3.2 MPa (Table 1) [47].

In order to verify that the bulk material properties for compressive modulus of PCL were consistent with the value of 120 MPa reported by Solvay, SLS processed solid PCL cylinders were mechanically tested in compression. Experimental data confirmed that the compressive modulus of the bulk PCL material was approximately 120 MPa (Table 1).

The strength and modulus for each scaffold were plotted against volume fraction for the purpose of relating compressive mechanical properties to volume fraction (Fig. 4). Both compressive modulus and compressive yield strength showed positive correlations with volume fraction, with R^2 values of 0.4634 and 0.7938, respectively.

3.3. Image-based FEA

Compressive moduli computed by FEA on the design STL files correlated well with the moduli measured experimentally (Fig. 5). However, the experimental moduli were roughly twice predicted computational moduli.

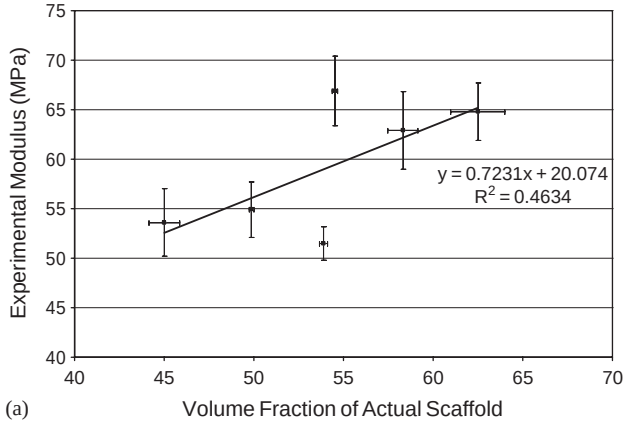

Fig. 4. Differences in correlation within (a) experimental modulus and volume fraction and (b) experimental yield strength and volume fraction are likely due to varying design geometries. A least-squares regression line is fit to the data to show correlation.

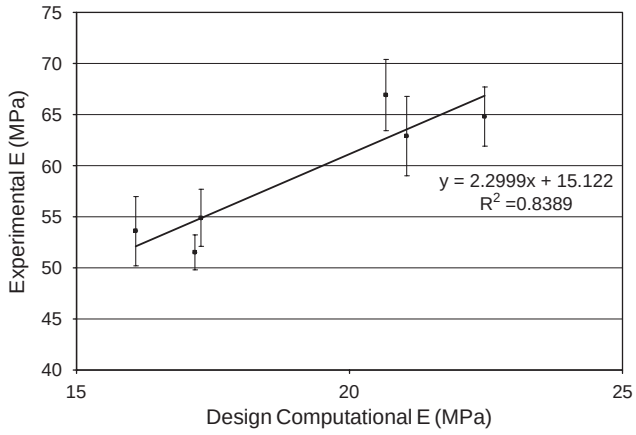

Fig. 5. Close correlation exists between the computational E value of each design file, and the experimental E value of the corresponding fabricated (actual) scaffolds. A least-squares regression line is fit to the data to show correlation.

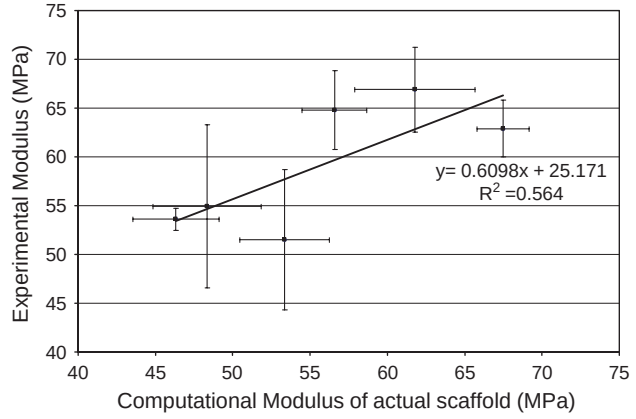

Fig. 6. Correlation between computational modulus of fabricated scaffolds and experimental modulus of fabricated (actual) scaffolds. A least-squares regression line is fit to the data to show correlation.

Image-based finite element (FE) models created directly from μCT scans of fabricated scaffolds did account for the increased volume fraction, and thus verified the ability of image-based FE models to compute scaffold stiffness prior to implantation without the need for destructive testing. Testing the actual PCL scaffolds both experimentally and computationally validates the computationally predicted compressive modulus data relative to the experimentally determined compressive modulus data. Fig. 6 demonstrates the correlation between computationally predicted modulus values of the different scaffold designs and their corresponding experimentally determined values.

3.4. Generation of bone in vivo

Micro-CT data indicated that 5.02 ($\pm$2.2) mm^3 of bone formed on or inside the orthogonal pore scaffolds

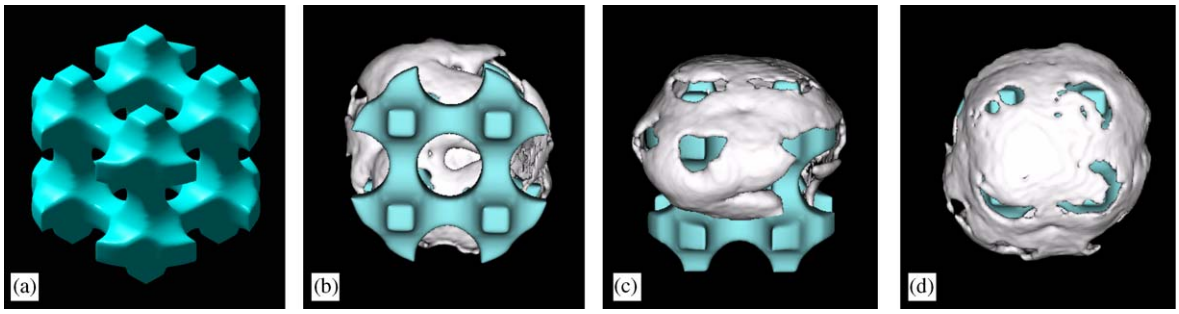

Fig. 7. (a) An isometric view of a surface rendering of the STL design file for the subcutaneous-size scaffold, (b) bottom view, (c) side view, (d) top view of μCT bone surface rendering data combined with a surface rendering of the STL design file. PCL scaffold is shown in blue and mineralized matrix is shown in white.

(initial scaffold volume = 99.5 mm^3). The volumetric bone mineral density (BMD) measures of the newly formed bone inside the scaffold pores or on the scaffold surfaces was 513.36 (±14.23) mg/cm^3. The BMD of the newly formed bone lies within the range of normal BMD measures of human trabecular and cortical bone, 120 and 1100 mg/cm^3, respectively [48]. Micro-CT images and bone surface renderings seen in Fig. 7 and Fig. 8a illustrate the newly formed bone that has grown onto and within a representative orthogonal pore scaffold after 4 weeks of implantation.

Histological staining confirmed the presence of bone reported by the μCT results. Fig. 8b shows a cortex surrounding the implant. Fig. 8c reveals the presence of normal bone morphology, including osteocytes, trabeculated structures, and marrow space. Large amounts of bone are shown around the exterior of the scaffold, as well as within the scaffold pores. Both μCT and histological staining reveal the presence of a cortex that enveloped the entire implant. Inside the "shell", marrow space and trabecular bone were observed both on the scaffold exterior and were penetrating into the scaffold pores (Fig. 8).

3.5. Mandibular condyle design and fabrication

The SLS fabrication technique successfully built mandibular condyle scaffolds designed using image-based design techniques. These scaffolds replicated the anatomy well (Fig. 9c and 9d) and could be built within 3 h.

4. Discussion

The fabrication of PCL scaffolds via SLS may ultimately result in a technique for the repair and regeneration of bone. The technique relies on the understanding that a skeletal reconstruction scaffold must possess mechanical properties that will support in

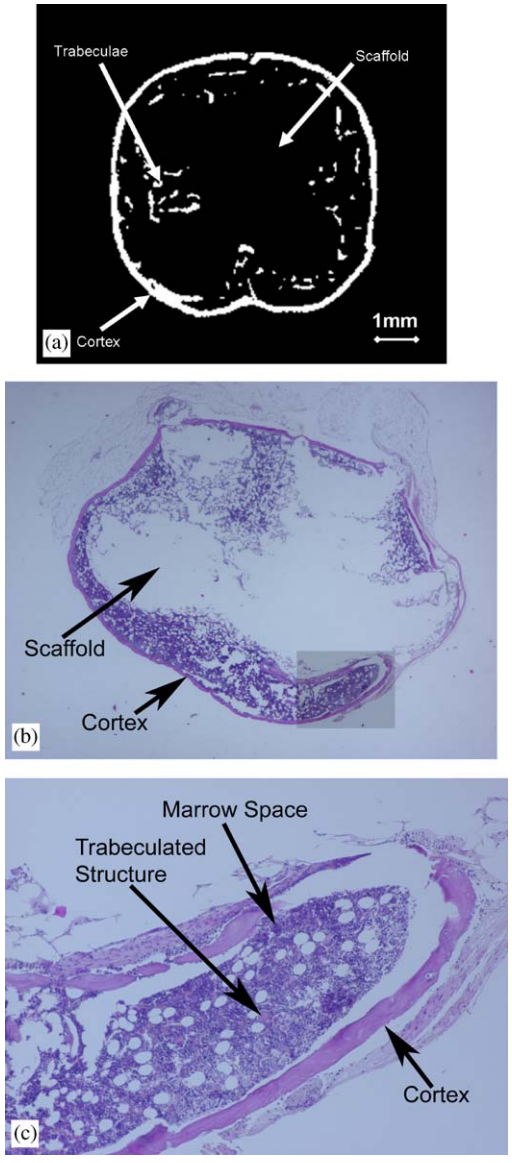

Fig. 8. (a) Top view of actual μCT data slice image (same orientation as 7d) shows cortical shell and areas of trabeculated structures within the marrow space that correspond to histological staining (H&E) shown in (b) and (c).

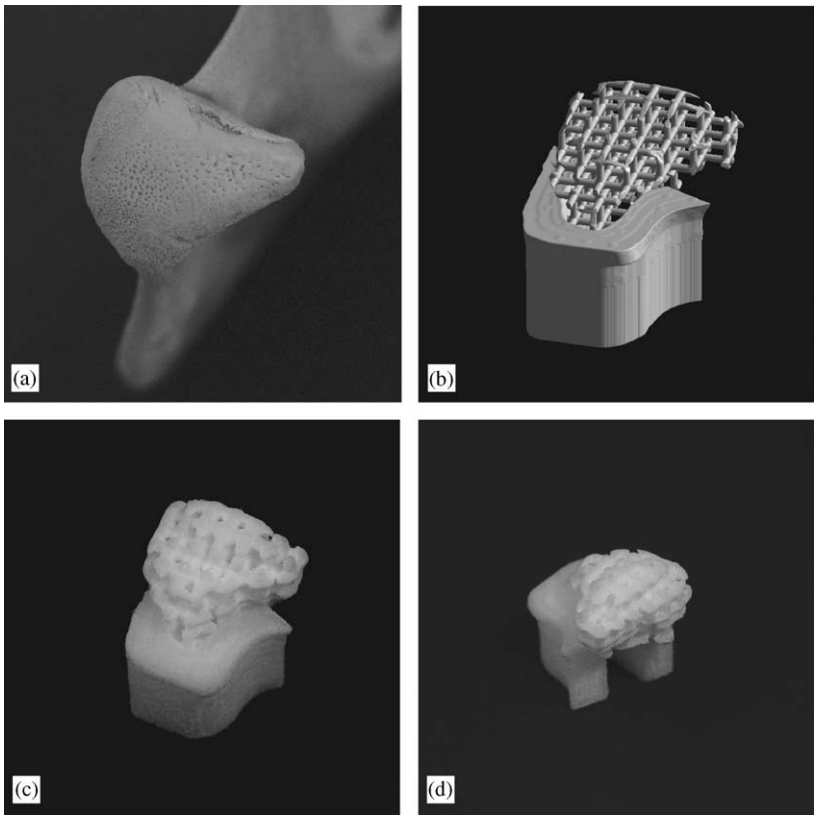

Fig. 9. (a) An actual pig condyle, (b) surface rendering of STL design file for pig condyle scaffold, (c) front view, and (d) back view of pig condyle PCL scaffold fabricated by SLS.

vivo loads, enhance tissue in-growth, produce biocompatible degradation byproducts, and fit anatomic defects [3–6]. Our results demonstrate that SLS fabricated scaffolds can satisfy these requirements. Furthermore, we have shown that computational analysis of these scaffolds can provide assessment of their mechanical properties without the need for destructive testing. The success in manufacturing the designed scaffolds, achieving appropriate mechanical characteristics of these scaffolds, and computationally analyzing these scaffolds, and their ability to support the in-growth of bone show the potential for use in tissue engineering.

Proper assessment of the mechanical properties of PCL scaffolds fabricated through SLS is necessary to ensure that the scaffold properties are within the range of human trabecular bone. Scaffold mechanical properties matching those of trabecular bone are important for early functional loading, which could also be beneficial to enhance bone formation and in-growth. [8]. Compressive modulus values of human trabecular bone range from 1 to 5000 MPa, with strength values ranging from 0.10 to 27.3 MPa [6,49–53] with mean values of approximately 194 and 3.55 MPa [47]. Our PCL scaffolds exhibit compressive modulus values ranging from 52 to 67 MPa and strength values ranging from 2.0 to 3.2 MPa, depending on scaffold porosity and geometry. Both these values fall within the lower range of human trabecular bone.

The integration of scaffold computational design and SFF techniques presented here could prove highly useful for the construction of scaffolds possessing patient specific anatomies and interior porous architectures derived from computational design optimizations. This process will not only enable the design of custom scaffold geometries, but by coupling design and fabrication with computational analyses, it will also enable us to predict the mechanical properties of specific implants without experimental testing. A correlation coefficient of 0.8611 exists between designed porosities and actual porosities of scaffolds (Fig. 3). This close correlation will enable fabrication of specific porosities by compensating for the fact that actual scaffold porosities differ from the designed porosities by the trend line reported ($y = 1.0324x - 27.854$), resulting in actual scaffolds with porosities that are 30–40% lower than designed porosities. The lower porosities seen in the actual scaffolds are due to excess PCL material trapped within the pores. For this reason, correlation between designed porosities and actual porosities should improve as SLS processing and post-process cleaning

methods improve. Next, the close correlation ($R^2 = 0.8389$) between computational modulus values of the design files and experimental modulus of the actual scaffolds (Fig. 5) will allow for computational determination of the mechanical properties of a particular design before it is manufactured. Finally, the correlation ($R^2 = 0.564$) that exists between the computational modulus of a fabricated porous scaffold and the experimental modulus of that same scaffold (Fig. 6), was lower than the correlation between designed and actual modulus. One major contributing factor to this lower correlation is excess material in the pores of the scaffold. Because the excess material does not have the same mechanical properties as the completely sintered material, it causes discrepancies in computational predictions. Once again, by improved processing parameters and better post-process cleaning methods, a closer correlation would be obtained between the computationally predicted modulus and the experimentally tested modulus. This would allow us to computationally assess the mechanical properties of the actual scaffold to be implanted, without having to experimentally test the scaffold.

As seen in Fig. 4, volume fraction of a scaffold does not completely predict the modulus value ($R^2 = 0.4634$). Modulus values calculated by FEA on the STL files for the different scaffold geometries versus volume fractions for the STL files also resulted in a low correlation ($R^2 = 0.5113$). This suggests that the differences in correlation result from differences in scaffold geometry, i.e. different packing of pores and different strut sizes. This will be important to consider in further studies of porous PCL scaffolds made through SLS.

We have shown, through μCT data and histology, that PCL scaffolds support bone regeneration in vivo via gene therapy. The cortex of bone surrounding marrow space that penetrated towards the interior of the scaffold, is similar to results obtained using other materials [54]. Furthermore, comparing μCT analysis and histological staining (Fig. 8) of the scaffolds revealed that μCT analysis provided adequate imaging of trabecular bone formation. Trabecular bone visualized by staining is also observed in the μCT scan. Micro-CT imaging of bone is advantageous in this application, as it allows for quantitative computations of bone regeneration.

It is essential to consider both the external shape and the internal architecture of the scaffold. Many groups have reported the manufacture of scaffolds with external shapes such as the ear [55,56], the aorta [57], or the nose [9] or of simple external shapes (i.e. cylinders or blocks) with intricate internal architectures [31,32,58,59]. Here, we show that SLS of PCL can produce scaffolds with both intricate external geometry and controlled internal architecture. By successfully fabricating a mandibular condyle scaffold implant (Fig. 9), we have demonstrated a method combining image-based computational design and SFF for producing biomimetic bone tissue engineering scaffolds in polycaprolactone.

While SLS provides many benefits in scaffold fabrication, there are certain limitations. The smallest attainable feature in SLS is primarily governed by the powder particle size, focused laser beam diameter and heat transfer in the powder bed. Larger particles increase the granularity of edges, layers and surfaces of parts produced by SLS. Yet, particles smaller than 10 μm exhibit poor flow and spreading properties. Smaller particles also sinter much faster when trapped inside scaffold pores and at boundaries of designed features, which causes dimensional inaccuracy from thermal growth and makes powder removal from pores or boundaries difficult. The optimal particle sizes for SLS processing are therefore in the 10–100 μm range. In the present commercial SLS machine embodiment, the Gaussian CO_2 laser beam is focused to a 450 μm spot which also theoretically limits the smallest SLS processed feature. In our experiments with PCL, the smallest pores that have been successfully fabricated are 1.75 mm in diameter. Experiments are ongoing to further optimize the SLS processing parameters and are anticipated to enable fabrication of scaffolds with yet smaller pores approaching the laser beam focal spot size.

5. Conclusions

PCL scaffolds fabricated via SLS show great potential for replacement of skeletal tissues. These scaffolds possess mechanical properties within the lower range of trabecular bone, suggesting they may have the ability to withstand early functional loading. PCL scaffolds fabricated by SLS can be easily manufactured to fit complex anatomic locations, demonstrated by, but not anatomically limited to, fabrication of a mandibular condyle. In vivo results show that SLS processed PCL scaffolds enhance tissue in-growth. Furthermore, the mechanical properties of these scaffolds can be computationally analyzed, bypassing the need for experimental testing. PCL scaffolds fabricated via SLS should prove advantageous for bone and cartilage tissue engineering in the future.

Acknowledgments

This work was funded by NIH grants DE 13608 (Bioengineering Research Partnership) and R21 DE 014736.

References

[1] Mercuri LG. Alloplastic temporomandibular joint reconstruction. Oral Surg Oral Med Oral Pathol Oral Radiol Endod 1998;85(6):631–7.

[2] Rutherford RB, Gu K, Racenis P, Krebsbach PH. Early events: the in vitro conversion of BMP transduced fibroblasts to chondroblasts. Connect Tissue Res 2003;44(1, Suppl 1):117–23.

[3] Agrawal CM, Ray RB. Biodegradable polymeric scaffolds for musculoskeletal tissue engineering. J Biomed Mater Res 2001;55(2):141–50.

[4] Das S, Hollister SJ. Tissue engineering scaffolds. In: Buschow KHJ, Cahn RW, Flemings MC, Ilschner B, Kramer EJ, Mahajan S, editors. Encyclopedia of materials: science and technology. Amsterdam: Elsevier; 2003.

[5] Griffith L. Polymeric Biomaterials. Acta Mater 2000;48:263–77.

[6] Langer R, Tirrell DA. Designing materials for biology and medicine. Nature 2004;428(6982):487–92.

[7] Taboas JM, Maddox RD, Krebsbach PH, Hollister SJ. Indirect solid free form fabrication of local and global porous, biomimetic and composite 3D polymer-ceramic scaffolds. Biomaterials 2003;24(1):181–94.

[8] Hutmacher DW. Scaffolds in tissue engineering bone and cartilage. Biomaterials 2000;21(24):2529–43.

[9] Landers R, Pfister A, Hubner U, John H, Schmelzeisen R, Mulhaupt R. Fabrication of soft tissue engineering scaffolds by means of rapid prototyping techniques. J Mater Sci 2002;37(15):3107–16.

[10] Sachlos E, Czernuska JT. Making tissue engineering scaffolds work. Review on the application of solid freeform fabrication technology to the production of tissue engineering scaffolds. Eur Cells Mater 2003;5:29–40.

[11] Sun W, Darling A, Starly B, Nam J. Computer aided tissue engineering part I: overview, scope, challenges. J Biotech Appl Biochem 2004;39(1):29–47.

[12] Sun W, Lal P. Recent development on computer aided tissue engineering-a review. Comp Method Prog Biomed 2002;67:85–103.

[13] Deckard CR. Part Generation by Layerwise Selective Sintering, MS thesis, Department of Mechanical Engineering, University of Texas at Austin; 1986.

[14] Deckard, CR. Selective Laser Sintering, PhD dissertation, Department of Mechanical Engineering, University of Texas at Austin; 1988.

[15] Berry E, Brown JM, Connell M, Craven CM, Efford ND, Radjenovic A, Smith MA. Preliminary experience with medical applications of rapid prototyping by selective laser sintering. Med Eng Phys 1997;19(1):90–6.

[16] Das S, Hollister SJ, Flanagan C, Adewunmi A, Bark K, Chen C, Ramaswamy K, Rose D, Widjaja E. Freeform fabrication of nylon-6 tissue engineering scaffolds. Rapid Prototyping J 2003;9(1):43–9.

[17] Shishkovsky IV, Tarasova EYu LV, Zhuravel LV, Petrov AL. The synthesis of a biocomposite based on nickel titanium and hydroxyapatite under selective laser sintering conditions. Techn Phys Lett 2001;27(3):211–3.

[18] Tan KH, Chua CK, Leong KF, Cheah CM, Cheang P, Abu Bakar MS, Cha SW. Scaffold development using selective laser sintering of polyetheretherketone-hydroxyapatite biocomposite blends. Biomaterials 2003;24(18):3115–23.

[19] Vail NK, Swain LD, Fox WC, Aufdlemorte TB, Lee G, Barlow JW. Materials for biomedical applications. Mater Design 1999;20(2–3):123–32.

[20] Azevedo MC, Reis RL, Claase MB, Grijpma DW, Feijen J. Development of polycaprolactone/hydroxyapatite composite biomaterials. J Mater Sci: Mater Med 2003;14:103–7.

[21] Cai Q, Bei J, Wang S. Synthesis and degradation of a tri-component copolymer derived from glycolide, L-lactide, and epsilon-caprolactone. J Biomater Sci Polym Ed 2000;11(3):273–88.

[22] Calvert JW, Marra KG, Cook L, Kumta PN, DiMilla PA, Weiss LE. Characterization of osteoblast-like behavior of cultured bone marrow stromal cells on various polymer surfaces. J Biomed Mater Res 2000;52(2):279–84.

[23] Fromstein JD, Woodhouse KA. Elastomeric biodegradable polyurethane blends for soft tissue applications. J Biomater Sci Polym Ed 2002;13(4):391–406.

[24] Guan J, Sacks MS, Beckman EJ, Wagner WR. Synthesis, characterization, and cytocompatibility of elastomeric, biodegradable poly(ester-urethane)ureas based on poly(caprolactone) and putrescine. J Biomed Mater Res 2002;61(3):493–503.

[25] Guan J, Sacks MS, Beckman EJ, Wagner WR. Biodegradable poly(ether ester urethane)urea elastomers based on poly(ether ester) triblock copolymers and putrescine: synthesis, characterization and cytocompatibility. Biomaterials 2004;25(1):85–96.

[26] Kweon H, Yoo MK, Park IK, Kim TH, Lee HC, Lee H-S, Oh J-S, Akaike T, Cho C-S. A novel degradable polycaprolactone networks for tissue engineering. Biomaterials 2003;24(5):801–8.

[27] Malinconico M, Immirzi B, Massenti S, La Mantia FP, Mormile L, Petti L. Blends of polyvinylalcohol and functionalized polycaprolactone: a study on the melt extrusion and post-cure of films suitable for protected cultivation. J Mater Sci 2002;37:4973–8.

[28] Mano JF, Koniarova D, Reis RL. Thermal properties of thermoplastic/starch synthetic polymer blends with potential biomedical applicability. J Mater Sci: Mater Medicine 2003;14:127–35.

[29] Marra KG, Szem JW, Kumta PN, DiMilla PA, Weiss LE. In vitro analysis of biodegradable polymer blend/hydroxyapatite composites for bone tissue engineering. J Biomed Mater Res 1999;47(3):324–35.

[30] Washburn NR, Simon Jr CG, Tona A, Elgendy HM, Karim A, Amis EJ. Co-extrusion of biocompatible polymers for scaffolds with co-continuous morphology. J Biomed Mater Res 2002;60(1):20–9.

[31] Hutmacher DW. Scaffold design and fabrication technologies for engineering tissues-state of the art future perspectives. J Biomater Sci Polymer Ed 2001;12(1):107–24.

[32] Hutmacher DW, Schantz T, Zein I, Ng KW, Teoh SH, Tan KC. Mechanical properties and cell culture response of polycaprolactone scaffolds designed and fabricated via fused deposition modeling. J Biomed Mater Res 2001;55(2):203–16.

[33] Rohner D, Hutmacher DW, Cheng TK, Oberholzer M, Hammer B. In vivo efficacy of bone-marrow-coated polycaprolactone scaffolds for the reconstruction of orbital defects in the pig. J Biomed Mater Res Part B: Appl Biomater 2003;66B: 574–80.

[34] Zein I, Hutmacher DW, Tan KC, Teoh SH. Fused deposition modeling of novel scaffold architectures for tissue engineering applications. Biomaterials 2002;23(4):1169–85.

[35] Wang F, Shor L, Darling A, Sun W, Guceri S, Lau A. Precision extruding deposition and characterization of cellular poly-e-caprolactone tissue scaffolds. Solid Freeform Fabrication Symposium Proceedings. University of Texas; 2003.

[36] Wu BM, Borland SW, Giordano RA, Cima LG, Sachs EM, Cima MJ. Solid free-form fabrication of drug delivery devices. J Controlled Release 1996;40(1–2):77–87.

[37] Xiong Z, Yan Y, Wang S, Zhang R, Zhang C. Fabrication of porous scaffolds for bone tissue engineering via low-temperature deposition. Scripta Materialia 2002;46(11):771–6.

[38] Sun W, Starly B, Darling A, Gomez C. Computer aided tissue engineering part II: application to biomimetic modeling and

design of tissue scaffolds. J Biotech Appl Biochem 2004;39(1): 49–58.
[39] Franceschi RT, Wang D, Krebsbach PH, Rutherford RB. Gene therapy for bone formation: in vitro and in vivo osteogenic activity of an adenovirus expressing BMP7. J Cell Biochem 2000;78(3):476–86.
[40] Gazit D, Turgeman G, Kelley P, Wang E, Jalenak M, Zilberman Y, Moutsatsos I. Engineered pluripotent mesenchymal cells integrate and differentiate in regenerating bone: a novel cell-mediated gene therapy. J Gene Med 1999;1(2):121–33.
[41] Krebsbach PH, Gu K, Franceschi RT, Rutherford RB. Gene therapy-directed osteogenesis: BMP-7-transduced human fibroblasts form bone in vivo. Hum Gene Ther 2000;11(8):1201–10.
[42] Lieberman JR, Le LQ, Wu L, Finerman GA, Berk A, Witte ON, Stevenson S. Regional gene therapy with a BMP-2-producing murine stromal cell line induces heterotopic and orthotopic bone formation in rodents. J Orthop Res 1998;16(3):330–9.
[43] Rutherford RB, Moalli M, Franceschi RT, Wang D, Gu K, Krebsbach PH. Bone morphogenetic protein-transduced human fibroblasts convert to osteoblasts and form bone in vivo. Tissue Eng 2002;8(3):441–52.
[44] Schek RM, Hollister SJ, Krebsbach PH. Delivery and protection of adenoviruses using biocompatible hydrogels for localized gene therapy. Mol Ther 2004;9(1):130–8.
[45] Hollister SJ, Levy RA, Chu TM, Halloran JW, Feinberg SE. An image-based approach for designing and manufacturing craniofacial scaffolds. Int J Oral Maxillofac Surg 2000;29(1):67–71.
[46] Hollister SJ, Maddox RD, Taboas JM. Optimal design and fabrication of scaffolds to mimic tissue properties and satisfy biological constraints. Biomaterials 2002;23(20):4095–103.
[47] Goulet RW, Goldstein SA, Ciarelli MJ, Kuhn JL, Brown MB, Feldkamp LA. The relationship between the structural and orthogonal compressive properties of trabecular bone. J Biomechanics 1994;27(4):375–89.
[48] Chen Q, Kaji H, Iu MF, Nomura R, Sowa H, Yamauchi M, Tsukamoto T, Sugimoto T, Chihara K. Effects of an excess and a deficiency of endogenous parathyroid hormone on volumetric bone mineral density and bone geometry determined by peripheral quantitative computed tomography in female subjects. J Clin Endocrinol Metab 2003;88(10):4655–8.
[49] Lang SM, Moyle DD, Berg EW, Detorie N, Gilpin AT, Pappas Jr NJ, Reynolds JC, Tkacik M, Waldron 2nd RL. Correlation of mechanical properties of vertebral trabecular bone with equivalent mineral density as measured by computed tomography. J Bone Jt Surg Am 1988;70(10):1531–8.
[50] Lotz JC, Gerhart TN, Hayes WC. Mechanical properties of trabecular bone from the proximal femur: a quantitative CT study. J Comput Assist Tomogr 1990;14(1):107–14.
[51] Mow VC, Hayes WC. Basic Orthopaedic Biomechanics. Philadelphia, PA: Lippincott-Raven Publishers; 1997. pp. 88–89.
[52] Ouyang J, Yang GT, Wu WZ, Zhu QA, Zhong SZ. Brief report: biomechanical characteristics of human trabecular bone. Clinical Biomechanics 1997;12(7/8):522–4.
[53] Porter BD, Oldham JB, He SL, Zobitz ME, Payne RG, An KN, Currier BL, Mikos AG, MJ Y. Mechanical properties of a biodegradable bone regeneration scaffold. J Biomech Eng 2000;122(3):286–8.
[54] Schek RM, Mazumder J, Holliser SJ, Krebsbach PH. Gene therapy from composite solid free form fabricated scaffolds. 2004; ORS Poster No: 0743.
[55] Cao Y, Vacanti JP, Paige KT, Upton J, Vacanti CA. Transplantation of chondrocytes utilizing a polymer-cell construct to produce tissue-engineered cartilage in the shape of a human ear. Plast Reconstr Surg 1997;100(2):297–302 (discussion 303–4).
[56] Yan Y, Rendong W, Zhang R, Xiong Z, Lin F. Biomaterial forming research using RP technology. Rapid Prototyping Journal 2003;9(3):142–9.
[57] Jockenhoevel S, Zund G, Hoerstrup SP, Chalabi K, Sachweh JS, Demircan L, Messmer BJ, Turina M. Fibrin gel—advantages of a new scaffold in cardiovascular tissue engineering. Eur J Cardio-Thoracic Surg 2001;19(4):424–30.
[58] Chu TM, Orton DG, Hollister SJ, Feinberg SE, Halloran JW. Mechanical and in vivo performance of hydroxyapatite implants with controlled architectures. Biomaterials 2002;23(5): 1283–93.
[59] Sherwood JK, Riley SL, Palazzolo R, Brown SC, Monkhouse DC, Coates M, Griffith LG, Landeen LK, Ratcliffe A. A three-dimensional osteochondral composite scaffold for articular cartilage repair. Biomaterials 2002;23(24):4739–51.